Int. J. Nano Dimens., 10 (4): 330-339, Autumn 2019

ORIGINAL ARTICLE

Synthesis of $MnFe_2O_4$ nanoparticles for adsorption of digestive enzymes: Kinetics, isothermal and thermodynamics studies

Adeogun Abideen Idowu [1,], Kareeem Sarafadeen Olateju [2], Adebayo Oluwatobi Samson [2]*

[1] *Chemistry Department, Federal University of Agriculture, Abeokuta, Nigeria*
[2] *Department of Microbiology, Federal University of Agriculture, Abeokuta, Nigeria*

Received 21 January 2019; revised 18 April 2019; accepted 02 May 2019; available online 05 May 2019

Abstract

The role of enzyme engineering in biotechnology, biological and pharmaceutical process cannot be over emphasized. This study compared the adsorption of amylase and protease on to manganese ferrite ($MnFe_2O_4$). The metal ferrite was synthesized via a sol – gel technique and characterized with scanning electron microscopy (SEM), X-ray diffraction (XRD), Electron paramagnetic resonance (EPR) and Fourier transform infrared spectroscopy (FTIR). The adsorption was study in a batch process and the data were subjected to kinetics and isotherm models. The pseudo-first order best fitted the kinetic data with $R^2 > 0.99$. The data were fitted well by the entire isotherm models considered with the maximum adsorption isotherm of 1.602 and 7.330 mg/g. The thermodynamic parameters give negative Gibb's free energy, ΔG, showing a spontaneous adsorption; positive ΔH indicated an endothermic favoured process, while ΔS values showed that the process progress with lower entropy change.

Keywords: *Adsorption; Amylase; Isotherm; Manganese Ferrite; Protease.*

How to cite this article

Abideen Idowu A, Sarafadeen Olateju K, Oluwatobi Samson A. Synthesis of MnFe2O4 nanoparticles for adsorption of digestive enzymes: Kinetics, isothermal and thermodynamics studies. Int. J. Nano Dimens., 2019; 10 (4): 330-339.

INTRODUCTION

Intrinsic surface activity of proteins could be attributed to presence and distribution of amphiphilic and amphoteric characteristics of polar, non-polar, acidic and basic side chains present in their structures. These lead to the formations of regions of different hydrophobicity and surface charges, hence, their marginal conformational stability in aqueous environments. Proteins spontaneous adsorptions in the presence of nearly all surfaces results from their electrochemical diversity and their conformational stability in aqueous environments [1]. The understanding of the adsorption process of proteins onto biomaterial surface is of great importance owing to the fundamental roles they played when in contact with inorganic surfaces in biological milieu. Also, understanding the mechanisms governing protein adsorption is pertinent to their wide range of applications in materials science which include; biofouling, biocatalysis, biosensing, drug release and separation of biomolecules [1–5]. Recent advances in the entrapment of proteins and other biological species into a wide range of sol-gel-derived nanocomposite materials and their use for biosensor and biological applications have been studied extensively [6, 7]. Their adsorption onto nanoparticles is influence by factors such as: nanoparticle material, size, shape, morphology, curvature, surface chemistry and change in protein (secondary and tertiary) structures which occur progressively with respect to time [7].

Enzymes are widely used industrially because of their high specificity, catalytic efficiency, low toxicity, biodegradability, mild operational conditions when compared with inorganic catalysts [8]. Amylase and protease belongs to the group of proteins known as technical enzymes due to their bulk applications in detergents, textile, organic synthesis, biofuels, and pulp and paper

* Corresponding Author Email: abuaisha2k3@yahoo.com

industries [9]. Owing to their wide applications, isolation, separation and purification of technical enzymes are of major concern.

Various techniques have been employed in enzyme immobilization/purification; these include chromatography, electrophoretic, ultrafiltration, precipitation and other procedures with affinity chromatography being one of the most important techniques [10, 11]. Although these are established procedures, they cannot be used for samples loaded with particulate material in the early stages of the isolation/purification process as found in enzymes. These techniques are not that simple and are also expensive when compared with adsorption technique which has higher commercial potential, simple and ability to retain high catalytic activity after adsorption. Furthermore, adsorption method offers the reusability of expensive supports after inactivation of immobilized enzyme [12, 13].

In this study, $MnFe_2O_4$ was synthesized via a sol – gel technique and characterized with scanning electron microscopy (SEM), electron diffraction analysis (EDAX), X-ray diffraction (XRD), Electron paramagnetic resonance (EPR) and Fourier transform infrared spectroscopy (FTIR). It was used for the adsorptions of α-amylase and protease. The kinetics data from their adsorptions studies were subjected to pseudo first order, second order, Elovich and intraparticule diffusion kinetic models. Similarly, data from equilibrium studies were analyzed with Guggenheim–Anderson–de Boer (GAB), generalized adsorption isotherms, Freudlich, Tempkin and Dubinin-Raduskevithch (D-R) adsorption isotherm models. The temperature dependent adsorption data were used for the estimation of the thermodynamic parameters.

MATERIALS AND METHODS

Materials

All chemical used in the study were analytical reagent grade, they were used without further purification. Ferric nitrate nanohydrate ($Fe(NO_3)_3.9H_2O$) and manganese nitrate hexahydrate ($Mn(NO_3)_2.4H_2O$) were from Sigma Aldrich, while citric acid and ammonium were obtained from British Drug Houses. MilliQ water was used for all of the experiments.

Synthesis of $MnFe_2O_4$ Nanoparticle

Manganese ferrite ($MnFe_2O_4$) was synthesized via a sol-gel technique by weighing accurately 0.25101 g of $Mn(NO_3)_2.4H_2O$ and 0.80799 g of $Fe(NO_3)_3.9H_2O$ and dissolved in 10 ml Milli Q water. The solutions of the salt were mixed, stirred at 60 ^oC for 12 hours after which citric acid was added as a chelating agent and further stirred at 90 ^oC till dark brown sol-gel is formed. A sudden increase in temperature led to the combustion resulting into the formation of $MnFe_2O_4$nanoparticles. The $MnFe_2O_4$ nanoparticle was calcinated at 800 ^oC for 4 hours and characterized by different physicochemical techniques.

Characterization of the synthesized $MnFe_2O_4$

Surface morphology and elemental composition of the material was analysed using scanning electron microscopy (SEM) [VEGA3 TESCAN], X-ray diffraction (XRD) data were collected using a PAN Analytical X' Pert PRO X-ray diffractometer with Cu Kα radiation (λ = 1.5418Å). Fourier transform infrared (FT-IR) spectra were recorded from 400 to 4000 cm^{-1} in TENSOR 27spectrometer (Bruker, Germany) using KBr pellet technique while the magnetic property were analysed with Bruker EMX Plus (Brucker, Germany) with Microwave Frequency of 9.859876, Modulation Frequency of 100.0 kHz and Modulation Amplitude of 1.0 G.

Isotherm and kinetic studies for the adsorption enzymes by $MnFe_2O_4$

Crude enzymes were obtained from Microbiology Laboratory, Federal University of Agriculture Abeokuta, Nigeria. Adsorptions of the enzymes (amylase and protease) onto the surface of $MnFe_2O_4$ were carried out as earlier described [14]. Briefly, 5ml of different concentrations (1.0 – 20.0 mg/L) of the crude enzyme was contacted with 0.002 g of the nanoparticle in a 10 ml vial at room temperature and pH 7.0. The final suspension was mixed for 30 seconds to disperse the nanoparticles and subsequently shaken for predetermined time on an orbital shaker. The adsorbed protein was separated from the mixture using an external magnetic field and the supernatant was analyzed for the protein content. The difference in protein concentration compared with the blank was as a result of enzyme adsorption on to the adsorbent. Adsorption kinetics was studied by determining the amount of protein in the supernatant by repeating the procedure above at different contact time. The amounts of enzyme adsorbed at time *t,* Q_t (mg/g) and at equilibrium Q_e (mg g) were calculated using equation 1 and 2 below:

$$Q_t = \frac{(C_o - C_t)V}{W} \quad (1)$$

$$Q_e = \frac{(C_o - C_e)V}{W} \quad (2)$$

Where C_o (mg/L) is the initial concentration and C_t (mg/L) is the concentration of the crude enzyme at time t in the liquid-phase. C_e (mg/L) is the concentration of the enzyme in the supernatant at equilibrium, *V* is the volume of the solution (L), and *W* is the mass of $MnFe_2O_4$.

Isotherm and kinetic modeling of adsorption process

The adsorption mechanisms of protease and amylase onto the $MnFe_2O_4$ were investigated by applying, pseudo-first order, pseudo-second order kinetic models [15], Elovich kinetics [16] and intraparticle diffusion [17] models to describe the kinetics of the adsorption process. Equations 3 – 6 represent the kinetics models, where Q_e is the amount of enzyme in mgg^{-1} adsorbed at equilibrium while k_1, *and* k_2 are the pseudo first order and pseudo-second order rate constants respectively. K_{di} is intraparticle diffusion constant while C_i measures the thickness of the particle layer. The Elovich parameters α and β_{el} are initial adsorption rate (mg/ g min)) and the desorption constant (g/mg) [14].

$$Q_t = Q_e(1 - e^{-k_1 t}) \quad (3)$$

$$Q_t = \frac{k_2 Q_e^{\,2} t}{1 + k_2 Q_e t} \quad (4)$$

$$Q_t = K_{di} * t^{0.5} + C_i \quad (5)$$

$$Q_t = {}^{1}\!/_{\beta_{el}} \ln(\alpha\beta_{el} * t) \quad (6)$$

Equilibrium data from the adsorption studies were also subjected to two (2) and three (3) parameters isotherm models. The two parameters isotherms are the Freundlich isotherm (Eqn. 7) which described the heterogeneity in the surface and Tempkin isotherm (Eqn. 8) which suggested a linear decrease in surface energy upon adsorption, taking into account the adsorbent/adsorbate interactions. The parameters K_F and *n* described adsorption capacity and intensity while, the constants a_T and b_T of the Tempkin model are related to equilibrium binding constant (*L/μg*) and the heat of adsorption. The three parameters models are: the Guggenheim–Anderson–de Boer (GAB), generalized adsorption isotherms, and Dubinin-Raduskevithch (D-R) adsorption isotherm models. GAB adsorption model (Eqn. 9) is a combination of two distinct adsorption states, i.e. equivalent adsorption site where the adsorbate bind strongly with the possibility of the occupied site successively adsorbed weakly to the adsorbate. The model reduces to Langmuir equation whenK_s= 0. L_k and K_s are respectively the weak and strong state adsorption constants, while Q_o is the maximum adsorption in the inner wall of the adsorbent [14, 18]. Generalized adsorption isotherm model (Eqn. 10) take into account the saturation of the binding site and cooperativity in the sites of adsorption. Cooperative binding constant, can be used to explain the trends of binding observable during adsorption, when m *value>1,* this implies an increase in affinity for other adsorbate molecule upon binding to one site while *m < 1* indicates that binding on one site reduces affinity of others site. However, when m value is unity (i.e. m = 1), it implies an independent binding of the adsorbent to available sites. K_G is the saturation constant in μgL^{-1} while Q_m is the maximum adsorption capacity [14].

$$Q_{eq} = K_F C_e^{\,1/n} \quad (7)$$

$$Q_e = \frac{RT}{b_T} \ln a_T C_e \quad (8)$$

$$Q_{eq} = \frac{Q_o L_K C_e}{(1 + L_K C_e - K_s C_e)(1 - K_S C_e)} \quad (9)$$

$$Q_{eq} = \frac{Q_m C_e^m}{(K_G + C_e^m)} \quad (10)$$

$$Q_e = Q_s Exp(-\beta\varepsilon^2) \quad (11)$$

The D–R sorption isotherm (Eqn. 11) is based on assumptions of equipotent of the adsorption sites, absence of stoic hindrance between adsorbed and incoming particles as well as surface homogeneity at microscopic level. The parameters Q_s is the theoretical saturation capacity ($mol\ g^{-1}$), β is a constant related to the mean free energy of adsorption per mole of the adsorbate ($mol^2\ J^{-2}$), and ε is the Polanyi potential given by the relation;

$\varepsilon = RT\ln(1+{}^{1}/_{C_e})$. C_e is the equilibrium concentration of enzyme (mg L^{-1}), R (J mol^{-1} K^{-1}) is the gas constant and T (K) is the absolute temperature. The constant β gives an idea about the mean free energy E (kJ mol^{-1}) of adsorption per molecule of the adsorbate when it is transferred to the surface of the solid from relationship. $E = (2\beta)^{-0.5}$ If the magnitude of E is between 8 and 16 kJ mol^{-1}, the process is chemisorption, while for values of E < 8 kJ mol^{-1} suggests a physical process.

Data analysis and Statistical Test

Non-linear regression analysis method using a program written on Micro Math Scientist software (Salt Lake City, Utah) was used to obtain the least square fit for all the models. The acceptability and the best fit of a model for linearized models are typically based on the square of the correlation coefficients, R^2. However, this study employed least square fit for the data modeling; therefore, error distribution comparison is desirable. Three error functions were used to validate the fit kinetic models, they are: the sum square errorfunction (SSE), root mean square error (RMSE) and composite fractional error (HYBRD)

$$SSE = \sum_{i=1}^{N} (Q_{(\exp)} - Q_{(cal)})^2 \quad (12)$$

$$RMSE = \sqrt{\frac{\sum_{i}^{N} (Q_{(\exp)} - Q_{(cal)})^2}{N}} \quad (13)$$

$$HYBRD = \frac{100}{N-P} \sum_{i}^{N} \frac{(Q_{(\exp)} - Q_{(cal)})}{Q_{(\exp)}} \quad (14)$$

Where *N* represents the number of data points and *P* are the numbers of the parameters in the model. The higher is the value of R^2 and the lower the value of SSE, RMSE and HYBRD errors the more acceptable the model.

RESULTS AND DISCUSSION

Characterizations of $MnFe_2O_4$

Fig. 1(a, b and c) shows the surface morphology and surface elemental composition of the $MnFe_2O_4$. SEM analysis showed a well-defined porous structure with interconnected pores

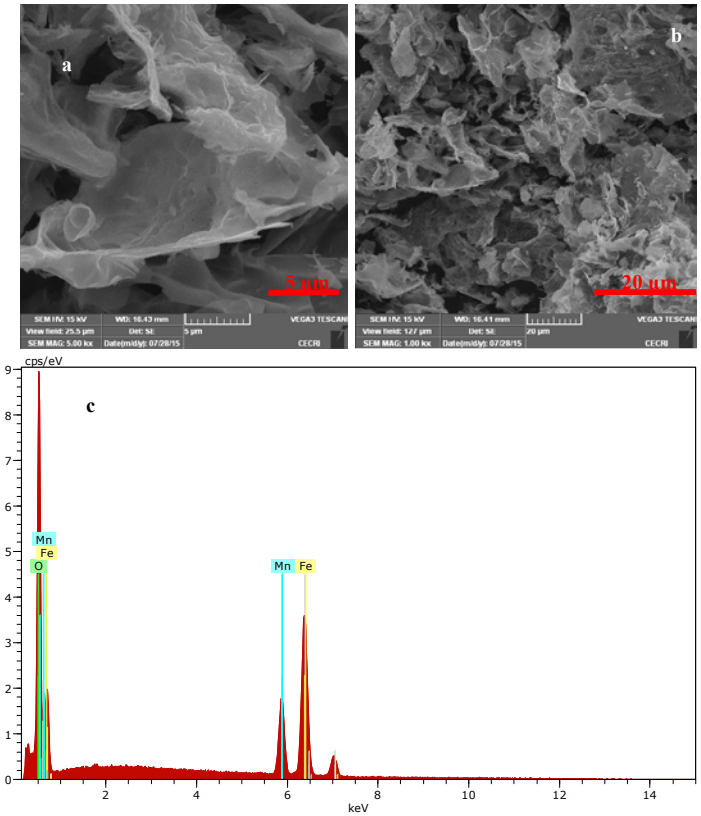

Fig. 1. The scanning electron micrograph (a, b) and energy diffraction X-ray (c) of $MnFe_2O_4$.

without evidence of a secondary phase. The energy dispersion X-ray analysis showed that the surface contains mainly Mn, Fe and O in the desired ratio.

The XRD patterns of $MnFe_2O_4$ is shown in Fig. 2 all diffraction peaks in the XRD patterns easily indexed to $MnFe_2O_4$ (JCPDS 10-0319) and compare satisfactorily to cubic spinel structure No other impurity peaks were noted which is a clear indication of pure product pure. Using Debye–Scherrer equation, $D = \frac{k\lambda}{\beta \cos\theta}$ for the strongest peaks, the mean grain sizes of ~ 5.11 nm was obtained.

The EPR spectra of $MnFe_2O_4$ were obtained at 9.859876 GHz, at room temperature to determine its magnetic properties. EPR study of $ZnFe_2O_4$ is presented in Fig. 3 and its parameters were determined using $g = \frac{h\nu}{\beta H}$. The value resonance width (ΔH) obtained from Lorentzian fit was 238.08 Gauss, while with resonance field of 3351 (Gauss) was obtained and the effective g- factor was estimated to be 2.08.

Figs. 4a and b show the FT-IR spectra of the $MnFe_2O_4$ before and after the adsorption of the enzyme. The prominent absorption bands characteristics of ferrites were noted below 1000 cm^{-1}, the peaks at 557 and 640 cm^{-1} are attributed to Fe-O and Mn-O bonds vibrations. The broad band at 3415cm^{-1} and peak at 1630 cm^{-1} are due to the vibration and stretching of O–H bond and upon enzyme adsorption, the band reduced drastically, signifying H-bonding of the enzyme with nanoparticle.

Kinetics and mechanism of adsorption

The adsorption kinetics study provides means of understanding pathways and mechanism of adsorption processes. Generally, adsorption processes are controlled by three diffusion steps i.e. transportation of the solute from bulk solution to the film surrounding the adsorbent, followed by transportation of the film to the adsorbent surface, and finally from the surface to the internal sites where the adsorbate bind to the active sites. The overall rate of the adsorption process is determined by the slowest step of all these steps [19]. The adsorption kinetic data obtained from the adsorption of α-amylase and protease enzymes by $MnFe_2O_4$ were subjected to kinetic model given by the Equations 3 to 6, Figs. 5 (a, b, c d and d) and 6 (a, b, c d and d) were obtained from the least square fit of the kinetic models, while Table 1 shows the parameter for the non linear fits of the models.The increase in the quantity of enzyme adsorbed *(Q_t)* increases with time and enzyme concentrations observed from the plots indicates gradual occupation of the empty

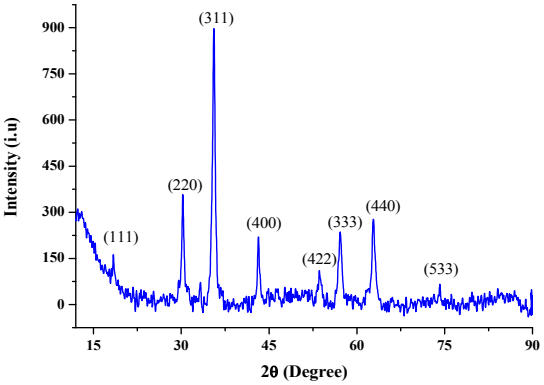

Fig. 2. XRD patterns of the $MnFe_2O_4$.

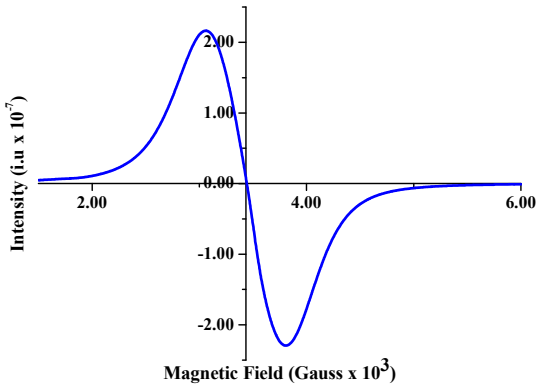

Fig. 3. EPR study of $MnFe_2O_4$.

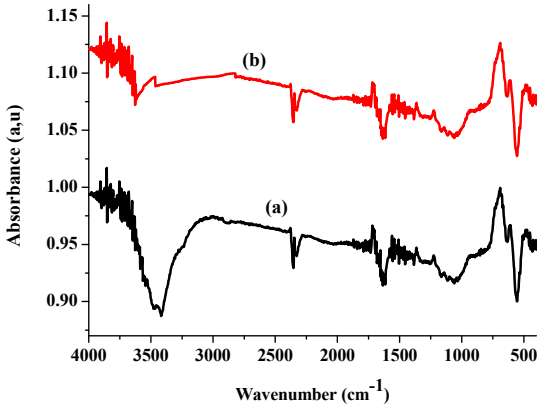

Fig. 4. FT-IR spectra of the $MnFe_2O_4$: (a) before and (b) after the adsorption.

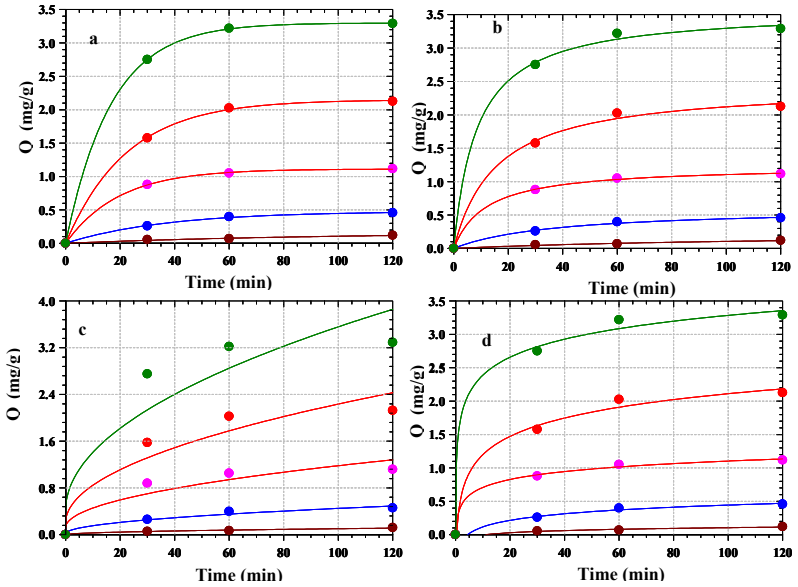

Fig. 5. Kinetic fits for the adsorption of α - amylase on $MnFe_2O_4$ (a) pseudo-first order model fits (b) pseudo-second order model fits (c) Intraparticle diffusion and (d) Elovich model fits.

Table 1. kinetic parameters for the adsorption of α-amylase and protease by $MnFe_2O_4$.

	C_o (µg/L	Amylase					Protease				
		1	2	`2.5	3	4	5	8	10	15	20
Pseudo-first order	$Q_{e(exp)}$ (mg/g)	0.119	0.456	1.116	2.125	3.29	0.76	2.023	4.822	8.431	12.834
	Q_e (mg/g)	0.09	0.479	1.112	2.149	3.299	0.768	1.947	4.76	8.311	12.614
	k_1(min^{-1})	0.019	0.027	0.051	0.045	0.06	0.032	0.041	0.042	0.058	0.075
	R^2	0.857	0.999	0.999	0.999	0.999	0.999	0.995	0.999	0.999	0.999
	%SSE	0.017	0.013	0.003	0.014	0.006	0.005	0.043	0.036	0.069	0.127
	RMSE	0.003	0.003	0.000	0.003	0.001	0.001	0.008	0.007	0.013	0.024
	HYBRD	4.603	-0.686	0.051	-0.160	-0.039	-0.149	0.558	0.186	0.206	0.249
Pseudo-second order	Q_e (mg/g)	0.248	0.609	1.237	2.448	3.577	0.933	2.263	5.503	9.096	13.377
	k_2 (g/(mgmin))	0.03	0.044	0.068	0.026	0.033	0.039	0.024	0.01	0.012	0.014
	R^2	0.955	0.998	0.999	0.999	0.999	0.999	0.997	0.999	0.999	0.999
	%SSE	0.074	0.088	0.07	0.187	0.166	0.1	0.139	0.393	0.384	0.313
	RMSE	0.014	0.017	0.013	0.036	0.032	0.019	0.027	0.076	0.074	0.060
	HYBRD	7.431	3.589	1.397	1.885	1.146	2.649	1.515	1.768	1.044	0.580
Intraparticle diffusion	k_{id}(mg /(gmin$^{0.5}$)	0.007	0.043	0.106	0.203	0.314	0.071	0.185	0.452	0.797	1.211
	C_{id} (mg/g)	0.018	0.016	0.12	0.202	0.415	0.042	0.152	0.397	0.993	1.775
	R^2	0.808	0.992	0.973	0.976	0.965	0.991	0.985	0.983	0.969	0.96
	%SSE	0.063	0.204	0.415	0.811	1.155	0.329	0.858	1.949	3.073	4.426
	RMSE	0.007	0.023	0.046	0.090	0.128	0.037	0.095	0.217	0.341	0.492
	HYBRD	7.522	6.406	5.318	5.453	5.016	6.186	6.057	5.775	5.206	4.927
Elovich	α (mg /(g min))	0.003	0.032	1.055	0.812	17.908	0.081	0.445	1.214	22.57	1432.291
	β_{el} (g /mg)	12.16	7.037	5.825	2.521	2.567	5.097	2.467	1.038	0.921	0.931
	R^2	0.999	0.998	0.999	0.999	0.999	0.999	0.999	0.999	0.999	0.999
	SSE	0.112	0.185	0.220	0.492	0.474	0.266	0.606	1.323	1.443	1.452
	RMSE	0.012	0.021	0.024	0.055	0.053	0.030	0.067	0.147	0.160	0.161
	HYBRD	214.878	9.710	3.516	4.300	2.403	7.704	6.117	5.399	2.951	1.822

sitesas the adsorption progressed and subsequent saturated at equilibrium.

The first order kinetic model has best fitted the kinetic data, with initial increase in rate constant as the initial enzyme concentration increases as shown in Figs. 5a and 6a. Although average values of R^2 obtained for both first and second order kinetic model (Figs 5b and 6b) are almost the same, first order was adjudged as the best fit owing to the values of Q_e obtained ($Q_{e,calc}$), which are consistent with the experimental values (Q_{eexp}). Furthermore, statistical error analysis with lower values of the %SSE, RMSEand HYBRD also in favour the first order model when compared with the second order parameters. The Elovich model fits (Figs 5c and 6c) and the parameters showed an increase in

adsorption rate, α and decreases desorption rate, *β* with increasing enzyme concentrations. This is attributed to increase the concentration gradient across the surface and formation of chemical bond between the enzymes and functional groups present within $MnFe_2O_4$. The mechanisms of the adsorption of enzymes to $MnFe_2O_4$ were investigated using intraparticle diffusion model. The increases in intraparticle diffusion constant, k_{di} as the enzyme concentration noted for both amylase and protease adsorption by $MnFe_2O_4$ are related to the influence of increase driving force and corresponding resistance of the surface boundary to the concentration gradient as the enzymes accesses the available sites on $MnFe_2O_4$. The non-zero positive value of the intercepts C_i (Figs 5d and 6d) showed that adsorption is not solely determined by intraparticle diffusion, rather mass transfer of the enzymes into the internal structure of the adsorbent also played significant roles [14].

Adsorption isotherms

The distribution of the adsorbate between the solid and liquid phases at equilibrium adsorption is studied using isotherm models for proper selection of suitable model for the design purpose. Equilibrium adsorption data of α-amylase and protease enzymes on $MnFe_2O_4$ were subjected to isotherm models given by the Equations 7 to 11,

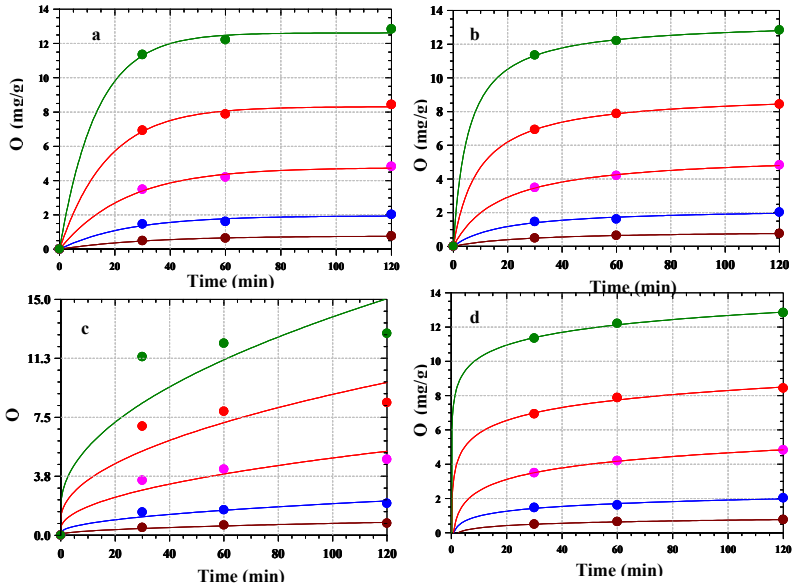

Fig. 6. Kinetic fits for the adsorption of protease on $MnFe_2O_4$ (a) pseudo-first order model fits (b) pseudo-second order model fits (c) Intraparticle diffusion and (d) Elovich model fits.

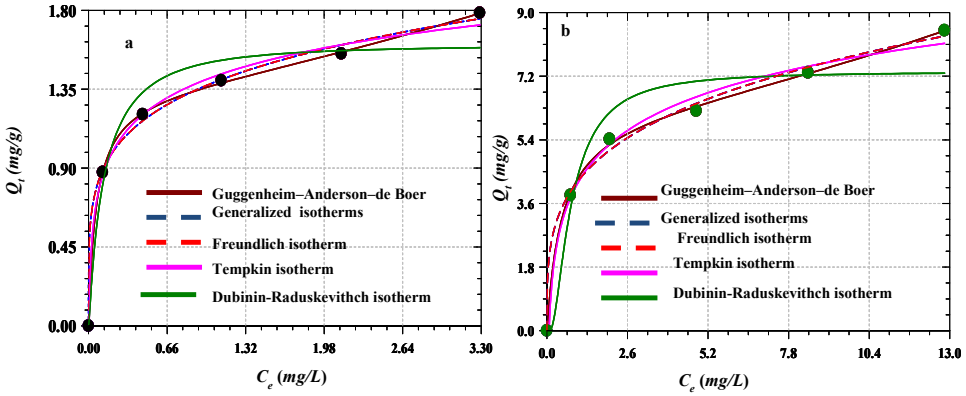

Fig. 7. Isotherm fits for the adsorption of enzymes onto $MnFe_2O_4$: (a) α-amylase (b) Protease.

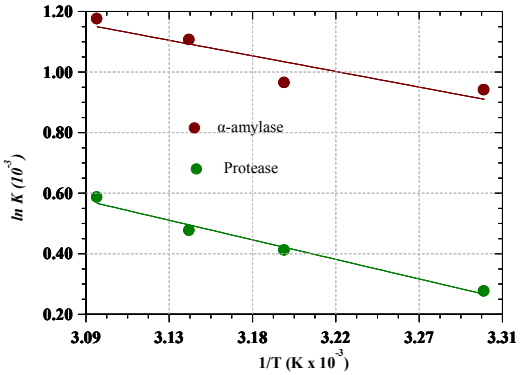

Fig. 8. van't Hoff plot of the adsorption of α-amylase and protease.

Table 2. Isotherm parameters for the adsorption of α-amylase and protease on $MnFe_2O_4$.

Isotherms	Parameters	α-Amylase	Protease
Guggenheim–Anderson–de Boer (GAB)	Q_{GAB} (mg/g)	1.325	6.114
	L_k(L /mg)	15.731	2.161
	K_s (L/mg)	0.081	0.023
	R^2	0.999	0.999
Generalized Adsorption Isotherm	Q_G (mg/g)	13.11	27.60
	K_G (L/mg)$^{1/m}$	9.53	6.51
	m	0.204	0.266
	R^2	0.999	0.999
Freudlich Isotherm	K_F (mg/(gmin$^{1/n}$))	1.374	4.233
	$1/n$	0.204	0.266
	R^2	0.999	0.999
Tempkin Isotherm	b_T	97.45	16.30
	a_T(L /g)	2.31.7	1.46
	R^2	0.999	0.998
R-D Isotherms	Q_S (mg/g)	1.602	7.330
	β x 10^8 (mol J^{-1})^2	2.151	1.676
	E(kJ mol^{-1})	4.822	5.460
	R^2	0.992	0.986

Figs. 7 (a and b) were obtained by the least square fit of the models with the parameters shown in Table 2.

The Guggenheim–Anderson–de Boer (GAB) adsorption parameters for the adsorption of α-amylase and protease are as shown in Table 2. Q_{GAB} represents the surface concentration of the strongly adsorbed protein with protease having higher concentration compared with α-amylase. The value of weak adsorption constant K_s, is lower compared with strong adsorption constant, L_k for the enzymes, this implied a stronger adsorption of the enzymes to $MnFe_2O_4$. The higher value of strong adsorption constant of amylase over that of protease may be attributed to the higher number of amino acid present in the amylase and its compactness compare to protease, creating ease of interaction with adsorbent. The values of m obtained for the adsorption of both enzymes are less than unity; this implies non-cooperativity with reduced affinity for enzyme upon binding on another site. The Freundlich isotherm parameters, 1/n values of less than 1 obtained for all bothenzymes showed that the process of adsorption is highly favoured. Tempkin isotherm parameters obtained shown that protease adsorption required lower energy, hence the maximum adsorption capacity obtained for this enzyme. Dubinin – Radushkevich model gave theoretical saturation capacities values $Q_{s,}$ of 1.602 and 7.330 mg/grespectively for the amylase and protease, the maximum adsorption energies, E, ranges between 4.82 and 5.46 kJ mol^{-1} showing that the process is physisorption dominated process.

Thermodynamics of the adsorption process

The thermodynamics parameters i.e. ΔG°, ΔH° and ΔS° were estimated using the following relation:

$$\Delta G^{o} = -RT \ln K_{d} \quad (15)$$

$$\ln K_{d} = \frac{\Delta S^{0}}{R} - \frac{\Delta H^{0}}{RT} \quad (16)$$

The equilibrium constant, $K_{d,}$ is obtained from the values of $m*Q_e/C_e$ at different temperature equilibrium study, where m is the mass of the adsorbent. van't Hoff plot of $\ln K_d$ against the reciprocal of temperature (1/T) gives a straight line with intercept as $\frac{\Delta S^0}{R}$ and slope as $\frac{\Delta H^0}{R}$.

The thermodynamic parameters obtained from the van't Hoff linear plots of $\ln K_d$ versus 1/T plot shown in Fig. 8 are presented in Table 3.

The distribution constant increases with temperature, i.e. as the temperature increases, the H-bond within the adsorbate and solvent decreases thereby promoting adsorbate-adsorbent interaction with accompanying increase pore diffusion [20]. The negative values of ΔG obtained indicate the spontaneous nature of adsorption of both enzymes by the nanoparticle, while positive values of enthalpy change (ΔH) shows that the adsorption process is endothermic in nature, and low values of change in entropy (ΔS) show that spontaneous adsorption of the enzymes was accompanying by no significant change in the entropy.

CONCLUSION

We have demonstrated a successful synthesis of $MnFe_2O_4$ with appreciable magnetic and porous network. The size of which was controlled by calcination at high temperature. The excellent magnetic responsiveness was exploited for the separation and adsorption of amylase and protease from aqueous solution. The adsorption rate increases with initial enzyme concentration and time. The kinetic was best explained with pseudo-first order kinetic model, the intraparticle diffusion revealed that mass transfer also play significant role. The adsorption isotherm best fitted by the Guggenheim–Anderson–de Boer isotherm, strong binding of the protein predominated the adsorption process and that there was no cooperativity in binding. The thermodynamic parameters showed that the process is spontaneous, endothermic in nature with no significant increase in entropy. $MnFe_2O_4$ has been successfully used as adsorbent for amylase and protease adsorption from their aqueous solutions.

ACKNOWLEDGEMENTS

This work benefitted immensely from the financial support in the form of grants from CSIR, for 12 months TWAS-CSIR Postdoctoral Fellowship, FR Number: 3240275035, awarded to Abideen Idowu Adeogun that enables part of this work to be carried out at the CECRI Pollution Control Division Laboratory. We are also he is thankful to the authority of the Federal University of Agriculture, Abeokuta, Nigeria for Granting the study leave to honor the fellowship.

CONFLICT OF INTEREST

The authors declare that they have no competing interests.

REFERENCES

1. Felsovalyi F., (2012), Mechanistic study of the adsorption and desorption of proteins on silica, *PhD Thesis*, Colombia University p.218.
2. Dolatshahi-Pirouz A., Rechendorff K., Hovgaard M. B., Foss M., Chevallier J., Besenbacher F., (2008), Bovine serum albumin adsorption on nano-rough platinum surfaces studied by QCM-D. *Colloids and Surf. B: Biointerf.* 66: 53–59.
3. Long D., Zhang R., Qiao W., Zhang L., Liang X., Ling L., (2009), Biomolecular adsorption behavior on spherical carbon aerogels with various mesopore sizes. *J. Colloid and Interf. Sci.* 331: 40–60.
4. Mavropoulos E., Costa A. M., Costa L. T., Achete C. A., Mello A., Granjeiro J. M., Rossi A., (2011), Adsorption and bioactivity studies of albumin onto hydroxyapatite surface. *Colloids and Surf. B: Biointerf.* 83: 1–9.
5. Bozgeyik K., Kopac T., (2016), Adsorption properties of arc produced multi walled carbon nanotubes for bovine serum Albumin. *Int. J. Chem. Reactor Eng.* 14: 549–558.
6. Hartman M., (2015), Ordered mesoporous materials for bioadsorption and biocatalysis. *Chem. Mater.* 17: 4577–4593.
7. Khan S., Gupta A., Verma N. C., Nandi C. K., (2015), Kinetics of protein adsorption on gold nanoparticle with variable protein structure and nanoparticle size. *J. Chem. Phys.* 143: 164701 –16470 9.
8. Taylor R. E., (1991), Protein Immobilization Fundamentals and Applications, *Marcel Dekker,* New York, p. 2.
9. Shuang L., Xiaofeng Y., Shuai Y., Muzi Z., Xiaoning W., (2012), Technology prospecting on enzymes: Application, marketing and engineering. *Comput. Struc. Biotechnol. J.* 2: 1–10.
10. Bornhorst J. A., Falke J. J., (2000), Purification of proteins using polyhistidine affinity tags. In *Methods in enzymology*. Academic Press. 326: 245-254.
11. Sharma N. M., Kumar S., Sawhney S. K., (2003), A novel method for the immobilization of tyrosinase to enhance stability. *Biotechnol. Applied Biochem.* 38: 137-141.
12. Gooding J. J., Hall E. A. H., (1996), Membrane properties of acrylate bulk polymers for biosensor applications. *Biosens. Bioelectron.* 11: 1031-1040.
13. Yildiz A., Gür A., (2007), Adsorption of phenol and chlorophenols on pure and modified sepiolite. *J. Serbian*

Chem. Soc. 72: 467-474.
14. Adeogun A. I., Kareeem S. O., Adebayo O. S., Balogun S. A., (2017), Comparative adsorption of amylase, protease and lipase on $ZnFe_2O_4$: Kinetics, isothermal and thermodynamics studies. *3 Biotechnol*. 7: 198-203.
15. Lagergren S., (1898), About the theory of so-called adsorption of soluble substances. *Kungligasvenska Vetenskaps Akademiens. Handlingar Band.* 24: 1–39.
16. Ho Y. S., Ng J. C. Y., McKay G., (2000), Kinetics of pollutant sorption by biosorbents: Review. *Sep. Purif. Methods*. 29: 189–232.
17. Badruzzaman M., Westerhoff P., Knappe D. R. U., (2004), Intraparticle diffusion and adsorption of arsenic onto granular ferric hydroxide (GFH). *Water Res.* 38: 4002-4012.
18. Meissner J., Prause A., Bharti B., Findenegg G. H., (2015), Characterization of protein adsorption onto silica nanoparticles: Influence of pH and ionic strength. *Colloid Polym. Sci.* 293: 3381-3391.
19. Wang H., Yuan X., Wu Y., Huang H., Zeng G., Liu Y., Wang X., Lin N., Qi Y., (2013), Adsorption characteristics and behaviors of graphene oxide for Zn (II) removal from aqueous solution. *Appl. Surf. Sci.* 279: 432-440.
20. Daoud F. B. O., Kaddour S., Sadoun T., (2010), Adsorption of cellulose *Aspergillus niger* on a commercial activated carbon: Kinetics and equilibrium studies. *Colloids Surf. B: Biointerf.* 75: 93–99.